Inorg. Chem. **2007**, *46*, 8182–8192

Spin-Crossover Behavior in Cyanide-Bridged Iron(II)–Silver(I) Bimetallic 2D Hofmann-like Metal–Organic Frameworks

M. Carmen Muñoz,[†] Ana B. Gaspar,[‡] Ana Galet,[†] and José A. Real*[,‡]

Departament de Física Aplicada, Universitat Politècnica de València, Camino de Vera s/n, 46022, València, Spain, and Institut de Ciencia Molecular/Departament de Química Inorgànica, Universitat de València, Edificios de Institutos de Paterna, P. O. Box 22085, 46071 València, Spain

Received March 30, 2007

Two new series of compounds formulated $\{Fe(3\text{-Xpyridine})_2[Ag(CN)_2]_2\}$ (X = F (**1**), Cl (**2**), Br (**3**), I (**4**)) and $\{Fe(3\text{-Xpyridine})_2[Ag(CN)_2][Ag(3\text{-Xpyridine})(CN)_2]\}\cdot 3\text{-Xpy}$ (X = Br (**5**), I (**6**)) have been synthesized and characterized. The six compounds are made up of stacking of slightly corrugated two-dimensional coordination polymers defined by sharing $\{Fe_4[Ag(CN)_2]_4\}_n$ motifs. The stacking is different for the two families. In compounds **1**–**4** the layers are organized by pairs displaying argentophilic interactions; the Ag···Ag distance was found to be in the interval 3.0–3.3 Å, while the Ag···Ag separation between two consecutive layers belonging to different pairs was found to be around 6 Å. Compounds **5** and **6** are isostructural with a crystal packing defined by an almost homogeneous distribution of layers separated by around 8.3 Å (referred to the Fe···Fe interlayer distance). Between the layers an uncoordinated 3-Xpyridine molecule is included. Another 3-Xpyridine molecule, which remains in the plane defined by the $\{Fe_4[Ag(CN)_2]_4\}_n$ windows, coordinates one silver atom. Both series display quite different properties; at 300 K, **1**–**4** are pale-yellow and display similar distorted $[FeN_6]$ octahedron cores characteristic of the iron(II) ion in the high-spin state. **1** and **2** undergo a two-step ($T^{(1)}_{1/2}$ = 96 K and $T^{(2)}_{1/2}$ = 162 K) and a 50% spin transition ($T_{1/2}$ = 106 K), respectively. Compounds **3** and **4** are high-spin compounds at ambient pressure. **5** and **6** are deep red in color at 300 K and undergo spin-crossover behavior at significantly higher temperatures $T_{1/2}$ = 306 and 261 K, respectively.

Introduction

During the last years our group has been interested in developing new coordination polymers made up of suitable cyanometalate complexes acting as bridging ligands, iron(II) ions, and additional organic ligands, which in some cases can also act as bridges. The goal was to investigate the spin-crossover (SCO) phenomenon[1] in the resulting metal−organic frameworks. The primary motivation for undertaking this work was to extend the SCO phenomenon to different kinds of 1−3D compounds that presumably could display more rigid network structures and consequently more cooperative spin transitions.[2] Another motivation was to take advantage of new opportunities that could arise from the incorporation of switchable SCO building blocks in the construction of such new metal−organic frameworks.[3] One obvious strategy is to combine SCO and porosity to get host−guest-dependent SCO in the network. In this respect, our group reported long ago the first example of a nanoporous SCO coordination polymer, $[Fe(bpe)_2(NCS)_2]\cdot CH_3OH$ (the ligand bpe, previously referred to as tvp, is bis(pyridyl)ethylene); the large pores were formed from the perpendicular interpenetration of two series of parallel stacking of 2D layers.[4a] More recently, using a similar

* To whom correspondence should be addressed. E-mail: jose.a.real@uv.es.
[†] Universitat Politècnica de València.
[‡] Universitat de València.

(1) (a) Goodwin, H. A. *Coord. Chem. Rev.* **1976**, *18*, 293. (b) Gütlich, P. *Struct. Bonding (Berlin)* **1981**, *44*, 83. (c) König, E. *Struct. Bonding (Berlin)* **1991**, *76*, 51. (d) König, E.; Ritter, G.; Kulshreshtha, S. K. *Chem. Rev.* **1985**, *85*, 219. (e) Gütlich, P.; Hauser, A.; Spiering, H. *Angew. Chem., Int. Ed. Engl.* **1994**, *33*, 2024. (f) Gütlich, P., Goodwin, H. A., Eds. In *Spin Crossover in Transition Metal Compounds. Top. Curr. Chem.* **2004**, *233*−*235*.

(2) Real, J. A.; Gaspar, A. B.; Niel, V.; Muñoz, M. C. *Coord. Chem. Rev.* **2003**, *236*, 121.
(3) Real, J. A.; Gaspar, A. B.; Muñoz, M. C. *Dalton Trans.* **2005**, 2062.
(4) (a) Real, J. A.; Andrés, E.; Muñoz, M. C.; Julve, M.; Granier, T.; Bousseksou, A.; Varret, F. *Science* **1995**, *268*, 265. (b) Halder, G. J.; Kepert, C. J.; Moubaraki, B.; Murray, K. S.; Cashion, J. D. *Science* **2002**, *298*, 1762.

10.1021/ic700607x CCC: $37.00
Published on Web 09/01/2007

strategy, Kepert and co-workers reported a single-crystal to single-crystal transformation involving reversible sorption−desorption of solvent and its influence in the spin state of the building blocks in the compound $[Fe(4,4'\text{-azpy})_2(NCS)_2]\cdot S$ (4,4′-azpy = 4,4′-azopyridine).[4b] In both examples, like in others using long rodlike bis-monodentate ligands, the spin crossover is not sufficiently cooperative.

In 1996 Kitazawa and co-workers synthesized the compound $\{Fe(pyridine)_2[Ni(CN)_4]\}$, which represents the first 2D Hofmann-like coordination polymer exhibiting SCO properties,[5] and 5 years later we synthesized the homologous derivatives of Pd(II) and Pt(II). The three compounds have similar cooperative SCO properties and characteristic change of color upon spin change.[6] The use of pyrazine instead of pyridine enabled us to increase not only the dimensionality of the resulting 3D $\{Fe(pyrazine)[M^{II}(CN)_4]\}$ (M^{II} = Ni, Pd, Pt) polymers but also their cooperativeness as well as their critical temperatures.[6] Furthermore, the SCO properties of the latter series depend dramatically on the number of guest solvent molecules allocated in the pores. It has been proved, for the Pt derivative, that the spin transition can be switched, within the hysteresis loop, irradiating the sample with a pulse of light at room temperature[7] and that its SCO properties remain after growing thin layers of this polymer on gold surfaces.[8] All these aspects are essential when one considers the possibility of using these materials for memory devices.

Similarly, reaction of the $[M^{I}(CN)_2]^-$ (M^{I} = Cu, Ag, Au) species with iron(II) ions in presence of the ligands 4,4′-bipyrimidine, pyrazine, bpe, pyrimidine, and 3-CN-pyridine have afforded a rich variety of 1-3D frameworks with interesting thermal, pressure, and light-induced SCO properties.[9] Continuing with this research line, here we extend our studies in iron(II) SCO coordination polymers to a new series of 2D frameworks formed from self-assembly of dicyanoargentate, 3-halopyridine (3-Xpy, where X = F, Cl, Br, and I), and iron(II) in methanol/water (1:1). Two different families of polymers have been isolated depending on the concentration of 3-Xpy used. Yellow crystals of general formula $\{Fe(3\text{-Xpy})_2[Ag(CN)_2]_2\}$ (X = F (**1**), Cl (**2**), Br (**3**), and I (**4**)) were formed from stoichiometric amounts. However, the presence of an excess of 3-Xpy favors the formation of red crystals of what, at first sight, could be considered as a "clathrate" modification of **3** and **4**, $\{Fe(3\text{-Xpy})_2[Ag(CN)_2][Ag(3\text{-Xpy})(CN)_2]\}\cdot 3\text{-Xpy}$ (X = Br (**5**) and I (**6**)). This "clathration" involves simultaneously three-coordination of a Ag atom in a specific $[Ag(CN)]^-$ ligand to afford the $[Ag(3\text{-Xpy})(CN)_2]^-$ species and inclusion of the free ligand 3-Xpy in the crystal.

Experimental Section

Materials. $FeCl_2\cdot 4H_2O$, 3-Xpy (X = F, Cl, Br, I), and $K[Ag(CN)_2]$ were purchased from commercial sources and used as received.

Preparation of 1−6. These compounds were synthesized from slow diffusion of two methanol−water (1:1) solutions, one containing a mixture (2 mL) of $FeCl_2\cdot 4H_2O$ (0.25 mmol, 50 mg) and 3-Xpy (0.5 mmol, 48.83 mg (X = F), 57.11 mg (X = Cl), 79.5 mg (X = Br), and 103 mg (X = I)) in one side of the H-shaped vessel. The other side contained 2 mL of a solution of $K[Ag(CN)_2]$ (0.5 mmol, 100 mg). The two solutions were communicated filling the H-shaped vessel with additional methanol−water solution (1:1). Pale-yellow crystals (**1**−**4**) were formed 2 weeks later. When an excess of 3-Brpy or 3-Ipy was used, red crystals of **5** and **6** were formed. All the manipulations were performed under an argon atmosphere. Anal. Calcd for $C_{14}H_8N_6F_2Ag_2Fe$ (**1**): C, 29.51; H, 1.42; N, 14.75. Found: C, 29.61; H, 1.45; N, 14.82 (yield ca. 30%). Calcd for $C_{14}H_8N_6Cl_2Ag_2Fe$ (**2**): C, 27.90; H, 1.34; N, 13.94. Found: C, 28.03; H, 1.38; N, 14.11 (yield ca. 30%). Calcd for $C_{14}H_8N_6Br_2Ag_2Fe$ (**3**): C, 24.31; H, 1.17; N, 12.15. Found: C, 24.41; H, 1.20; N, 12.31 (yield ca. 65%). Calcd for $C_{14}H_8N_6I_2Ag_2Fe$ (**4**): C, 21.40; H, 1.03; N, 10.70. Found: C, 21.48; H, 1.06; N, 10.73 (yield ca. 50%). Calcd for $C_{24}H_{16}N_8Br_4Ag_2Fe$ (**5**): C, 28.61; H, 1.60; N, 11.12. Found: C, 28.72; H, 1.65; N, 11.17 (yield ca. 15%). Calcd for $C_{24}H_{16}N_8I_4Ag_2Fe$ (**6**): C, 24.11; H, 1.35; N, 9.37. Found: C, 24.11; H, 1.38; N, 9.42 (yield ca. 75%).

Magnetic Measurements. The variable-temperature magnetic susceptibility measurements were carried out on samples constituted of small single crystals (20−30 mg) using a Quantum Design MPMS2 SQUID susceptometer equipped with a 5.5 T magnet and operating at 1 T and 1.8−400 K. The susceptometer was calibrated with $(NH_4)_2Mn(SO_4)_2\cdot 12H_2O$. Experimental susceptibilities were corrected for diamagnetism of the constituent atoms by the use of Pascal's constants.

X-ray Crystallography. Diffraction data on prismatic crystals of **1**, **3**, and **4** were collected at 293 K while **2** and **6** were collected at two temperatures (270, 100 K and 270, 200 K, respectively) with a Nonius Kappa-CCD single-crystal diffractometer using Mo Kα (λ = 0.71073 Å). A multiscan absorption correction was performed but not applied. The absorption correction was found to have no significant effect on the refinement results. The structures were solved by direct methods using SHELXS-97 and refined by full-matrix least-squares on F^2 using SHELXL-97.[10] All non-hydrogen atoms were refined anisotropically. Relevant crystallographic data for **1**−**4** and **6** is displayed in Tables 1and 2.

Results

Crystal Structures. The crystal structures of compounds **1**−**4** and **6** have been investigated. Single crystals of **5** were not good enough to complete the whole data collection;

(5) Kitazawa, T.; Gomi, Y.; Takahashi, M.; Takeda, M.; Enemoto, A.; Miyazaki, T.; Enoki, T. *J. Mater. Chem.* **1996**, *6*, 119.
(6) Niel, V.; Martinez-Agudo, J. M.; Muñoz, M. C.; Gaspar, A. B.; Real, J. A. *Inorg. Chem.* **2001**, *40*, 3838.
(7) Bonhommeau, S.; Molnár, G.; Galet, A.; Zwick, A.; Real, J. A.; McGarvey, J. J.; Bousseksou, A. *Angew. Chem., Int. Ed.* **2005**, *44*, 4069.
(8) Cobo, S.; Molnár, G.; Real, J. A.; Bousseksou, A. *Angew. Chem., Int. Ed.* **2006**, *45*, 5786.
(9) (a) Niel, V.; Muñoz, M. C.; Gaspar, A. B.; Galet, A.; Levchenko, G.; Real, J. A. *Chem.—Eur. J.* **2002**, *8*, 2446. (b) Niel, V.; Galet, A.; Gaspar, A. B.; Muñoz, M. C.; Real, J. A. *Chem. Commun.* **2003**, 1248. (c) Niel, V.; Thompson, A. L.; Muñoz, M. C.; Galet, A.; Goeta, A. E.; Real, J. A. *Angew. Chem., Int. Ed.* **2003**, *42*, 3760. (d) Galet, A.; Niel, V.; Muñoz, M. C.; Real, J. A. *J. Am. Chem. Soc.* **2003**, *125*, 14224. (e) Galet, A.; Muñoz, M. C.; Martínez, V.; Real, J. A. *Chem. Commun.* **2004**, 2268. (f) Niel, V.; Thompson, A. L.; Goeta, A. E.; Enachescu, C.; Hauser, A.; Galet, A.; Muñoz, M. C.; Real, J. A. *Chem.—Eur. J.* **2005**, *11*, 2047. (g) Galet, A.; Gaspar, A. B.; Muñoz, M. C.; Bukin, G. V.; Levchenko, G.; Real, J. A. *Adv. Mater.* **2005**, *17*, 2949. (h) Galet, A.; Muñoz, M. C.; Gaspar, A. B.; Real, J. A. *Inorg. Chem.* **2005**, *44*, 8749. (i) Galet, A.; Muñoz, M. C.; Real, J. A. *Inorg. Chem.* **2006**, *45*, 4583. (j) Galet, A.; Muñoz, M. C.; Real, J. A. *Chem. Commun.* **2006**, 4321.
(10) Sheldrick, G. M. *SHELX97: Program for Crystal Structure Determination*; University of Gottingen: Gottingen, Germany, 1997.

Table 1. Crystal Data for **1**−**3**[a]

param	**1**	**2** (270 K)	**2** (100 K)	**3**
empirical formula	$C_{14}H_8N_6F_2Ag_2Fe$	$C_{14}H_8N_6Cl_2Ag_2Fe$		$C_{14}H_8N_6Br_2Ag_2Fe$
M_r	569.86	602.76		691.68
cryst system	triclinic	monoclinic		monoclinic
space group	$P\bar{1}$	$P2_1/c$		$P2_1/c$
a (Å)	10.6450(4)	9.2580(2)	9.1087(2)	9.4500(3)
b (Å)	12.3660(5)	12.9500(3)	12.6860(3)	12.5440(3)
c (Å)	15.0310(8)	16.5700(4)	16.3140(4)	16.8530(5)
α (deg)	99.888(2)			
β (deg)	93.642(2)	99.437(2)	99.696(2)	101.2430(10)
γ (deg)	95.419(3)			
V (Å^3)	1934.09(15)	1959.71(8)	1858.20(8)	1959.43(10)
Z	4	4		4
D_c (mg cm^{-3})	1.957	2.043	2.155	2.345
F(000)	1088	1152		1296
μ(Mo Kα) (mm^{-1})	2.771	2.990	3.153	6.797
cryst size (mm)	0.04 × 0.06 × 0.07	0.02 × 0.02 × 0.04		0.04 × 0.09 × 0.09
no. of tot. reflcns	7548	4473	4224	4484
no. of reflcns [$I > 2\sigma(I)$]	4260	3179	3498	3444
R_1 [$I > 2\sigma(I)$]	0.0618	0.0361	0.0341	0.0359
wR [$I > 2\sigma(I)$]	*0.1498*	*0.1040*	*0.0878*	*0.0894*
S	0.961	1.048	1.040	1.056

[a] $R_1 = \Sigma||F_o| - |F_c||/\Sigma|F_o|$. $wR = [\Sigma[w(F_o^2 - F_c^2)^2]/\Sigma[w(F_o^2)^2]]^{1/2}$; $w = 1/[\sigma^2(F_o^2) + (mP)^2 + nP]$, where $P = (F_o^2 + 2F_c^2)/3$, $m = 0.0975$ (**1**), 0.0691 (**2** HS), 0.0525 (**2** LS), and 0.0557 (**3**), and $n = 2.7179$ (**1**), 2.3348 (**2** HS), 6.8480 (**2** LS), and 1.8744 (**3**).

Table 2. Crystal Data for **4** and **6**[a]

param	**4**	**6** (270 K)	**6** (200 K)
empirical formula	$C_{14}H_8N_6I_2Ag_2Fe$	$C_{24}H_{16}N_8I_4Ag_2Fe$	
M_r	785.65	1195.64	
cryst system	monoclinic	monoclinic	
space group	$C2/c$	$P2_1$	
a (Å)	16.7860(7)	15.5780(2)	15.3630(4)
b (Å)	12.8930(6)	13.5570(2)	13.4180(3)
c (Å)	19.1560(10)	16.7680(3)	16.6060(5)
α (deg)			
β (deg)	97.442(2)	112.5781(6)	112.5030(10)
γ (deg)			
V (Å^3)	4110.9(3)	3269.84(9)	3162.53(14)
Z	8	4	
D_c (mg cm^{-3})	2.539	2.429	2.511
F(000)	2880	2192	
μ(Mo Kα) (mm^{-1})	5.596	5.428	5.612
cryst size (mm)	0.08 × 0.09 × 0.10	0.02 × 0.04 × 0.04	
no. of tot. reflcns	4422	14 021	13 737
no. of reflcns [$I > 2\sigma(I)$]	2590	11 331	9334
R_1 [$I > 2\sigma(I)$]	0.0491	0.0999	0.0984
wR [$I > 2\sigma(I)$]	0.1114	0.2954	0.2769
S	0.925	1.300	1.089

[a] $R_1 = \Sigma||F_o| - |F_c||/\Sigma|F_o|$. $wR = [\Sigma[w(F_o^2 - F_c^2)^2]/\Sigma[w(F_o^2)^2]]^{1/2}$; $w = 1/[\sigma^2(F_o^2) + (mP)^2 + nP]$, where $P = (F_o^2 + 2F_c^2)/3$, $m = 0.0712$ (**4**), 0.2000 (**6** (270 K)), and 0.1845 (**6** (200 K)), and $n = 5.3858$ (**4**), 0.0000 (**6** (270 K)), and 30.3463 (**6** (200 K)).

however, these partial data unambiguously indicated that it is isostructural to **6** (see Supporting Information). Compounds **2** and **3** are isostructural to each other. All these compounds define two-dimensional (2D) coordination polymers made up of $\{[Fe[Ag(CN)_2]_2]\}_\infty$ grids decorated with 3-Xpy motifs. Relevant crystallographic data as well as bond lengths and angles are gathered in Tables 1−4, respectively.

Structure of 1. This compound displays a two-step spin transition with $T_{1/2} = 95$ K and $T_{1/2} = 162$ K. However, unfortunately, these single crystals lose quality at low temperatures, a fact that prevented a full structural analysis at temperatures below 293 K. It crystallizes in the $P\bar{1}$ space group. The layers are made up of two crystallographically independent pseudooctahedral Fe(II) sites connected by four crystallographically independent almost linear $[Ag(CN)_2]^-$ units (Figure 1). These units are related by means of an inversion center placed between the layers. The Fe(1) and Fe(2) sites are rather similar with four cyanide moieties occupying the equatorial positions of the $[FeN_6]$ chromophores. The axial positions are occupied by two 3-Fpy groups, which adopt with respect to the relative position of the F atoms a *transoid* and a *cisoid* conformation for Fe(1) and Fe(2), respectively. The average Fe−N axial bond distances are virtually identical for both sites [2.225(5) Å] while the corresponding equatorial bond distances differ slightly being 2.157(9) and 2.149(8) Å for sites Fe(1) and Fe(2), respectively. These bond distances are consistent with the magnetic measurements at 293 K. The four independent $[Ag(CN)_2]^-$ units are also very similar and display an almost linear geometry; the C−Ag−C bond angle is in the 174.1(4)−179(4)° range. The units N(3)−C(11)−Ag(1)−C(27)−N(11) and N(5)−C(13)−Ag(2)−C(25)−N(9) connect in an

Table 3. Selected Bond Lengths (Å) and Angles (deg) for **1**−**4**

		2			
param	**1**	270 K	100 K	**3**	**4**
Fe(1)−N(1)	2.216(5)	2.234(4)	2.139(4)	2.245(4)	2.261(6)
Fe(1)−N(2)	2.234(5)	2.255(4)	2.127(4)	2.244(4)	2.260(7)
Fe(1)−N(3)	2.160(8)	2.149(4)	2.040(4)	2.149(4)	2.159(6)
Fe(1)−N(4)	2.156(7)	2.160(4)	2.058(4)	2.162(4)	2.170(6)
Fe(1)−N(5)	2.164(9)	2.142(4)	2.051(4)	2.158(4)	2.156(6)
Fe(1)−N(6)	2.148(7)	2.155(4)	2.048(4)	2.154(4)	2.147(6)
Fe(2)−N(7)	2.223(6)				
Fe(2)−N(8)	2.229(5)				
Fe(2)−N(9)	2.160(9)				
Fe(2)−N(10)	2.144(7)				
Fe(2)−N(11)	2.164(8)				
Fe(2)−N(12)	2.127(7)				
Ag(1)−C(11)	2.059(10)				
Ag(1)−C(27)	2.074(11)				
Ag(2)−C(13)	2.053(11)				
Ag(2)−C(25)	2.045(11)				
Ag(3)−C(12)	2.048(9)				
Ag(3)−C(14)	2.044(9)				
Ag(4)−C(26)	2.040(10)				
Ag(4)−C(28)	2.079(9)				
Ag(1)−C(11)		2.064(5)	2.059(5)	2.064(4)	2.055(8)
Ag(1)−C(14)		2.072(5)	2.071(5)	2.071(5)	2.055(8)
Ag(2)−C(12)		2.069(5)	2.077(5)	2.077(4)	2.070(8)
Ag(2)−C(13)		2.057(5)	2.068(5)	2.073(4)	2.083(8)
N(1)−Fe(1)−N(2)	177.8(2)	177.1(2)	177.3(2)	176.90(13)	176.0(2)
N(1)−Fe(1)−N(3)	92.4(3)	89.4(2)	90.4(2)	91.7(2)	93.2(2)
N(1)−Fe(1)−N(4)	90.5(3)	88.6(2)	91.6(2)	92.02(14)	84.5(2)
N(1)−Fe(1)−N(5)	86.7(3)	88.6(2)	91.5(2)	90.5(2)	92.5(2)
N(1)−Fe(1)−N(6)	87.6(3)	91.1(2)	88.8(2)	88.7(2)	90.6(2)
N(2)−Fe(1)−N(3)	88.8(3)	91.7(2)	88.6(2)	87.9(2)	88.2(2)
N(2)−Fe(1)−N(4)	91.4(3)	88.7(2)	90.9(2)	91.0(2)	91.9(2)
N(2)−Fe(1)−N(5)	92.1(3)	90.3(2)	89.5(2)	89.9(2)	91.3(2)
N(2)−Fe(1)−N(6)	90.6(3)	91.6(2)	88.69(14)	88.3(2)	88.2(2)
N(3)−Fe(1)−N(4)	89.4(3)	88.9(2)	87.2(2)	86.2(2)	86.0(2)
N(3)−Fe(1)−N(5)	178.5(3)	177.9(2)	178.1(2)	177.7(2)	90.8(2)
N(3)−Fe(1)−N(6)	88.6(3)	93.2(2)	90.7(2)	90.6(2)	175.6(3)
N(4)−Fe(1)−N(5)	91.7(3)	90.5(2)	93.1(2)	94.5(2)	175.4(3)
N(4)−Fe(1)−N(6)	177.2(3)	177.8(2)	177.8(2)	176.70(14)	96.5(2)
N(5)−Fe(1)−N(6)	90.2(3)	87.3(2)	89.1(2)	88.7(2)	86.9(2)
N(7)−Fe(2)−N(8)	176.7(2)				
N(7)−Fe(2)−N(9)	92.2(3)				
N(7)−Fe(2)−N(10)	92.9(3)				
N(7)−Fe(2)−N(11)	85.4(3)				
N(7)−Fe(2)−N(12)	90.8(3)				
N(8)−Fe(2)−N(9)	90.9(3)				
N(8)−Fe(2)−N(10)	88.3(3)				
N(8)−Fe(2)−N(11)	91.5(3)				
N(8)−Fe(2)−N(12)	88.1(2)				
N(9)−Fe(2)−N(10)	88.3(3)				
N(9)−Fe(2)−N(11)	177.2(3)				
N(9)−Fe(2)−N(12)	90.2(3)				
N(10)−Fe(2)−N(11)	90.3(3)				
N(10)−Fe(2)−N(12)	176.1(3)				
N(11)−Fe(2)−N(12)	91.4(3)				
C(11)−Ag(1)−C(27)	177.1(4)				
C(13)−Ag(2)−C(25)	176.8(4)				
C(12)−Ag(3)−C(14)	179.4(4)				
C(26)−Ag(4)−C(28)	174.1(4)				
C(11)−Ag(1)−C(14)		175.5(2)	174.8(2)	174.2(2)	177.8(3)
C(12)−Ag(2)−C(13)		176.6(2)	175.0(2)	174.8(2)	178.2(3)

alternate way the Fe(1) and Fe(2) sites forming infinite chains running parallel to the unit cell's diagonal ([0$\bar{1}$1] direction) (Figure 2). In contrast, the N(4)−C(12)−Ag(3)−C(14)−N(6) and N(10)−C(26)−Ag(4)−C(28)−N(12) bridges connect only one type of iron(II), site Fe(1) and Fe(2), respectively. Thus, the resulting infinite chains run perpendicularly ([100] direction) to the chains defined by the Ag(1) and Ag(2) sites. Hence, a grid-layered structure is formed. One edge of the almost rectangular $[FeAg(CN)_2]_4$ moiety is exactly the *a* cell parameter (10.6450(4) Å) and corresponds to the distances

Table 4. Selected Bond Lengths (Å) and Angles (deg) for **6**

param	270 K	200 K
Fe(A)−N(1A)	2.048(7)	2.008(10)
Fe(A)−N(2A)	2.070(8)	1.998(10)
Fe(A)−N(3A)	2.006(13)	1.92(2)
Fe(A)−N(4A)	2.037(13)	1.92(2)
Fe(A)−N(5A)	2.010(14)	1.933(9)
Fe(A)−N(6A)	1.968(12)	1.94(2)
Fe(B)−N(1B)	2.067(8)	1.971(10)
Fe(B)−N(2B)	2.063(8)	2.013(9)
Fe(B)−N(3B)	2.01(2)	1.93(2)
Fe(B)−N(4B)	2.070(14)	1.95(2)
Fe(B)−N(5B)	2.015(14)	1.97(2)
Fe(B)−N(6B)	2.008(13)	1.92(2)
Ag(1A)−C(11A)	2.08(2)	2.09(2)
Ag(1A)−C(14A)	1.95(2)	2.06(2)
Ag(2A)−C(12A)	2.11(2)	2.09(2)
Ag(2A)−C(13A)	2.08(2)	2.08(2)
Ag(1B)−C(11B)	2.01(2)	2.06(2)
Ag(1B)−C(14B)	2.07(2)	2.05(2)
Ag(2B)−C(12B)	2.100(14)	2.10(2)
Ag(2B)−C(13B)	2.13(2)	2.11(2)
N(1A)−Fe(A)−N(2A)	178.9(4)	179.5(6)
N(1A)−Fe(A)−N(3A)	90.3(4)	89.9(6)
N(1A)−Fe(A)−N(4A)	90.8(5)	90.0(6)
N(1A)−Fe(A)−N(5A)	90.2(5)	91.0(7)
N(1A)−Fe(A)−N(6A)	91.0(4)	90.2(6)
N(2A)−Fe(A)−N(3A)	90.8(5)	90.5(6)
N(2A)−Fe(A)−N(4A)	89.4(5)	90.3(6)
N(2A)−Fe(A)−N(5A)	88.7(5)	88.6(7)
N(2A)−Fe(A)−N(6A)	88.9(4)	89.5(6)
N(3A)−Fe(A)−N(4A)	91.5(5)	92.8(7)
N(3A)−Fe(A)−N(5A)	177.8(6)	178.4(9)
N(3A)−Fe(A)−N(6A)	88.7(5)	88.2(7)
N(4A)−Fe(A)−N(5A)	90.6(5)	88.5(8)
N(4A)−Fe(A)−N(6A)	178.3(6)	179.0(8)
N(5A)−Fe(A)−N(6A)	89.1(5)	90.5(8)
N(1B)−Fe(B)−N(2B)	178.3(4)	178.2(6)
N(1B)−Fe(B)−N(3B)	88.6(5)	89.6(6)
N(1B)−Fe(B)−N(4B)	90.2(5)	91.9(6)
N(1B)−Fe(B)−N(5B)	89.9(5)	92.0(6)
N(1B)−Fe(B)−N(6B)	88.1(5)	88.4(6)
N(2B)−Fe(B)−N(3B)	89.9(5)	89.0(6)
N(2B)−Fe(B)−N(4B)	90.7(5)	89.3(6)
N(2B)−Fe(B)−N(5B)	91.6(5)	89.4(6)
N(2B)−Fe(B)−N(6B)	91.1(5)	90.4(6)
N(3B)−Fe(B)−N(4B)	90.5(6)	91.4(8)
N(3B)−Fe(B)−N(5B)	178.3(6)	178.4(8)
N(3B)−Fe(B)−N(6B)	91.3(6)	89.5(7)
N(4B)−Fe(B)−N(5B)	88.8(6)	88.9(7)
N(4B)−Fe(B)−N(6B)	177.5(6)	179.1(8)
N(5B)−Fe(B)−N(6B)	89.3(5)	90.3(7)
C(11A)−Ag(1A)−C(14A)	172.3(7)	175.3(9)
C(12A)−Ag(2A)−C(13A)	161.8(6)	161.5(9)
C(11B)−Ag(1B)−C(14B)	174.4(7)	175.1(9)
C(12B)−Ag(2B)−C(13B)	160.7(6)	161.8(9)

Fe(2)···Fe(2) and Fe(1)···Fe(1), while the other side, which corresponds to the edge Fe(1)···Fe(2), is in average 10.583(2) Å. The angles defined by two consecutive edges Fe(2)···Fe(2)···Fe(1) and Fe(2)···Fe(1)···Fe(1) are respectively 95.5(6) and 84.5(6)°. The layers are corrugated as the Fe−N−C moieties in the Fe(2)···Ag(2)···Fe(1) edges are tilted forming angles notably smaller than 180° (i.e. Fe(1)−N(5)−C(13) = 164.3(8)° and Fe(2)−N(9)−C(25) = 164.7(8)°). Interestingly, the layers are organized by pairs, in which strong argentophilic interactions hold them together. The Ag···Ag distances in the double layer are Ag(1)···Ag(4^i) = 3.1026(10) Å (i = 2 − *x*, 1 − *y*, 1 − *z*) and Ag(2)···Ag(3) = 3.1681(11) Å. The double layers are organized in such a way that the iron atoms of one layer are below/above the

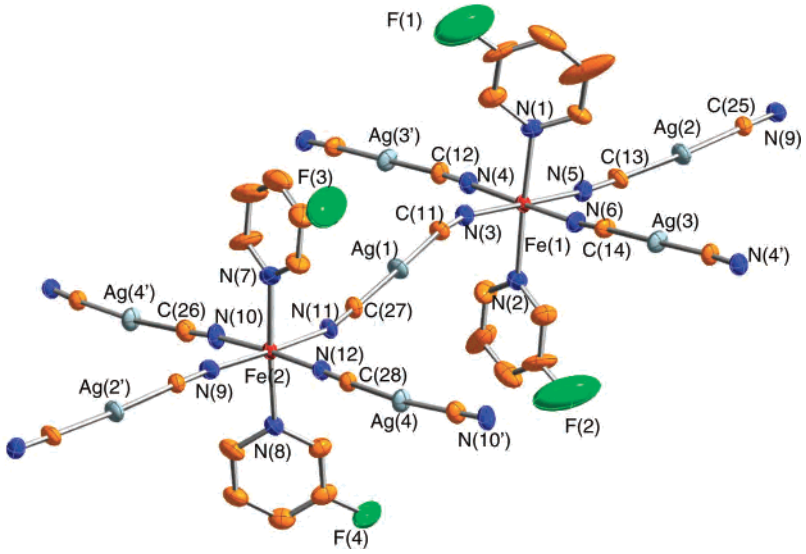

Figure 1. ORTEP representation of a fragment of **1** containing its asymmetric unit and atom numbering. Thermal ellipsoids are presented at 30% probability.

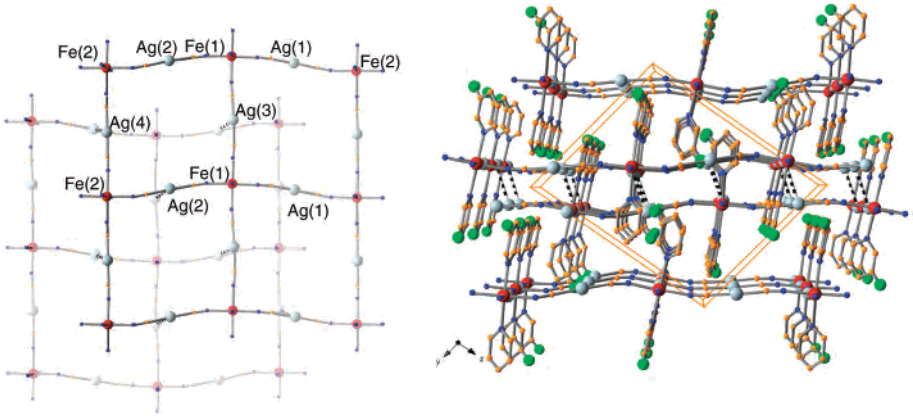

Figure 2. Left: View of the relative disposition of two grids of **1** emphasizing the argentophilic interactions (dotted bars). Right: Stacking of four consecutive layers of **1** along the [100] direction.

center of the windows defined by the other layer. These argentophilic contacts are placed at the center of the edges of the rhombuses (Figure 2). The distances between two consecutive non interacting layers are notably larger (Ag(2)···Ag(4^{ii}) = 6.2945(11) Å (ii = 2 − *x*, 1 − *y*, −*z*) and Ag(1)···Ag(3^{iii}) = 5.4424(11) Å (iii = *x*, *y* − 1, *z*)).

Structures of 2 and 3. Both derivatives are isostructural and crystallize in the monoclinic $P2_1/c$ space group. Compound **2** undergoes a 50% spin transition; consequently, its crystal structure has been investigated at temperatures above (270 K) and below (100 K) the critical temperature $T_c \approx$ 107 K. Compound **3** is HS, and its crystal structure has been studied at 293 K. Given that **2** is fully HS (high spin) at 270 K, its structure will be described together with that of **3**. There is only one crystallographically independent Fe(II) site. The iron(II) atom is surrounded by six nitrogen atoms belonging to two axial 3-Xpy (X = Cl, Br) ligands and four equatorial CN groups belonging to two crystallographically independent $[Ag(CN)_2]^-$ bridging groups. The axial Fe−N bond distances [Fe−N(1) = 2.234(4) (2.245(4)) Å; Fe−N(2) = 2.255(4) (2.244(4)) Å] are larger than the equatorial ones [Fe−N(3) = 2.149(4) (2.149(4)) Å; Fe−N(4) = 2.160(4) (2.162(4)) Å; Fe−N(5) = 2.142(4) (2.158(4)) Å; Fe−N(6) = 2.155(4) (2.154(4)) Å] for **2** and **3** (in parentheses), respectively (Figure 3).

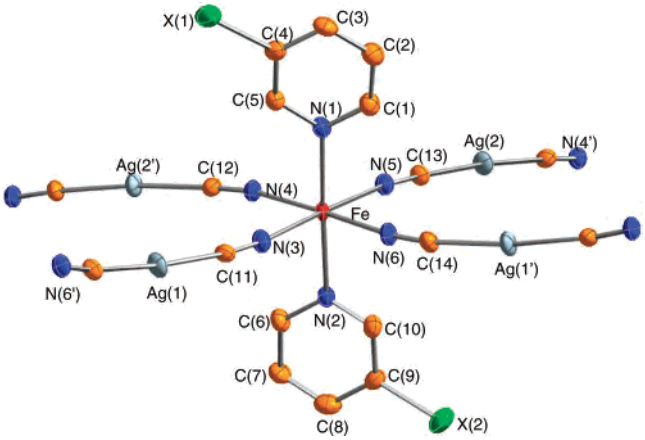

Figure 3. ORTEP representation of a fragment of **2** and **3** containing their asymmetric units and corresponding atom numbering. Thermal ellipsoids are presented at 30% probability.

Both $[Ag(CN)_2]^-$ groups have similar geometrical characteristics like those described for **1** and connect two Fe atoms defining a system of parallel 2D layers slightly more corrugated than in **1** (Figure 4). The intermetallic short

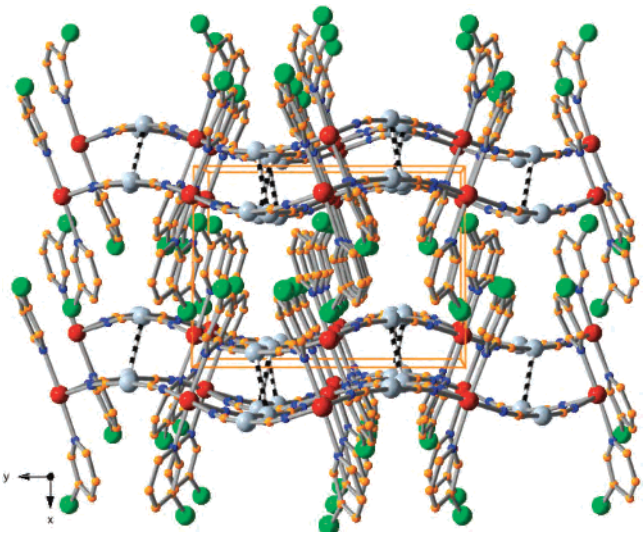

Figure 4. Stacking of four consecutive layers of **2** and **3** along the [001] direction.

distances in the double layers is Ag(1)···Ag(2^i) = 3.1181(7) and 3.1439(6) Å (i = 2 − *x*, 1 − *y*, −*z*) while it is 6.2593(7) Å (i = 1 − *x*, 1 − *y*, −*z*) and 6.4585(6) Å (i = *x* − 1, *y*, *z*) between two adjacent double layers for **2** and **3**, respectively. The $[FeAg(CN)_2]_4$ grids are much more distorted in **1**. The Fe−NCAg(1)CN−Fe and Fe−NCAg(2)CN−Fe edges are 10.566(2) and 10.464(2) Å for **2** and 10.435(2) and 10.574(2) Å for **3**, respectively. The average angle defined by two axes formed by the $[Ag(1 \text{ or } 2)(CN)_2]^-$ linker is 104.0(2)° (107.7(2)°), while the average angle determined by two edges defined by different Ag atoms is 76.4(2)° (73.3(2)°) for **2** (**3**).

The crystal structure of **2** at 100 K is essentially the same like at 270 K. However, significant structural changes associated with the spin conversion have been observed. The most noticeable change takes place in the $[FeN_6]$ coordination core. The average axial Fe−N bond distance shortens by 0.111 Å, and the corresponding equatorial one, by 0.102 Å. The total average is 0.105 Å and agrees quite well with what is expected for a half-spin transition in an iron(II) complex. This change of electronic configuration at the iron(II) has a notable influence in the structure of the [N(4)−C(12)−Ag(2)−C(13)−N(5)]$^-$ bridging ligand and less markedly in the [N(3)−C(11)−Ag(1)−C(14)−N(6)]$^-$ anion. For instance, the C(13)−N(5) and C(13)−Ag(2) bonds increase by 0.01 and 0.011 Å, respectively, while the N(4)−C(12) bond increases by 0.025 Å in the LS (low spin) state. These bond length variations are probably related with the increase of the Fe→N≡C−Ag π-back-bonding due to the increase of population of the dπ orbitals in the LS state. Noticeable bond angle variations are also observed during the change of spin state; particularly significant are Fe−N(3)−C(11) = 2.5°, Fe−N(6)−C(14) = 2.6°, N(3)−C(11)−Ag(1) = 5°, N(6)−C(14)−Ag(1) = 6.8°, N(4)−C(12)−Ag(2) = 4.3°, and N(5)−C(13)−Ag(2) = 4.1°. The size and shape of the $[FeAg(CN)_2]_4$ grids change as a consequence of these bond and angles variations. At 100 K the dimensions are 10.273(2) × 10.393(2) Å and the angles are 104.3(2) and 75.3(2)°.

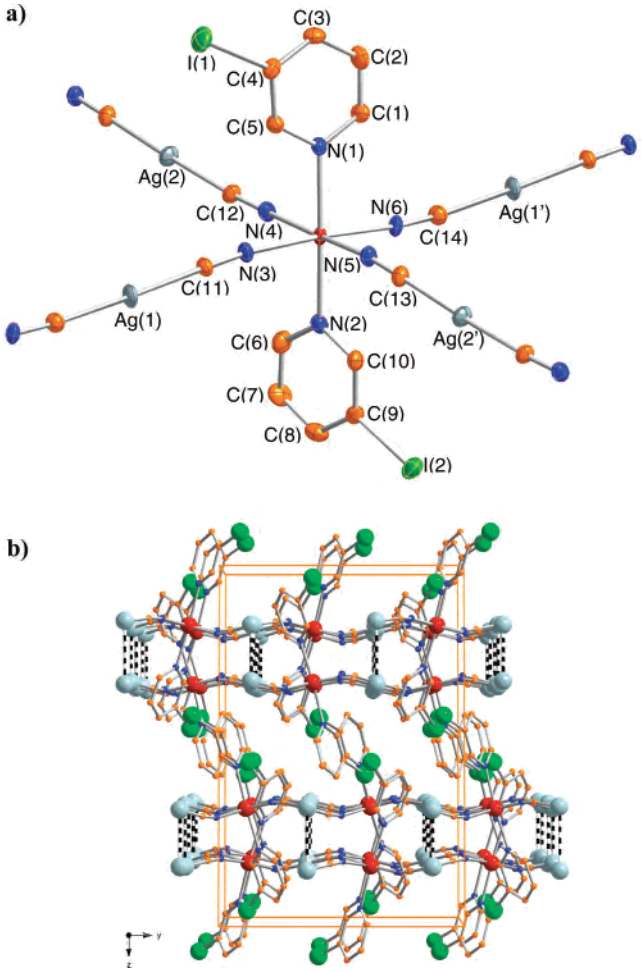

Figure 5. (a) ORTEP representation of a fragment of **4** containing its asymmetric unit and atom numbering. (b) Stacking of four consecutive layers of **4** along the [100] direction.

The Ag(1)···Ag(2^i) distance in the double layer and between double layers becomes slightly smaller as a consequence of the spin conversion, 3.0638(5) Å (i = 1 − *x*, −*y* − 1, 2 − *z*) and 6.1657(5) Å (i = 2 − *x*, −*y* − 1, −*z*), respectively.

Structure of 4. This compound crystallizes in the monoclinic *C*2/*c* space group. Its structure is very similar to that of **2** and **3**. As in the case of the latter compounds, there is only one type of iron(II) ion crystallographically independent (Figure 5a). This iron atom is in a pseudooctahedral environment with the 3-Ipy ligands in the axial positions [Fe−N(1) = 2.261(6) and Fe−N(2) = 2.260(7) Å] and two different $[Ag(CN)_2]^-$ coordinating the equatorial positions [Fe−N(3) = 2.159(6), Fe−N(4) = 2.170(6), Fe−N(5) = 2.156(6), and Fe−N(6) = 2.147(6) Å]. Both $[Ag(CN)_2]^-$ anions are almost linear [C(14)−Ag(1)−C(11) = 177.8(3) and C(13)−Ag(2)−C(12) = 178.2(3)°] and connect the iron atoms defining, similarly to **1**−**3**, a 2D polymeric structure made up of edge-sharing $\{Fe[Ag(CN)_2]\}_4$ rhombuses whose edge and angles are 10.583(7) Å and 75.0(3) and 104.9(3)°, respectively. The layers are organized by pairs in which two different types of argentophilic interactions are observed: Ag(1)···Ag(1^i) = 3.2727(11) Å and Ag(2)···Ag(2^{ii}) = 2.9635(11) Å (i = −*x*, *y*, $^1/_2$ − *z* and ii = 1 − *x*, *y*, $^1/_2$ − *z*,

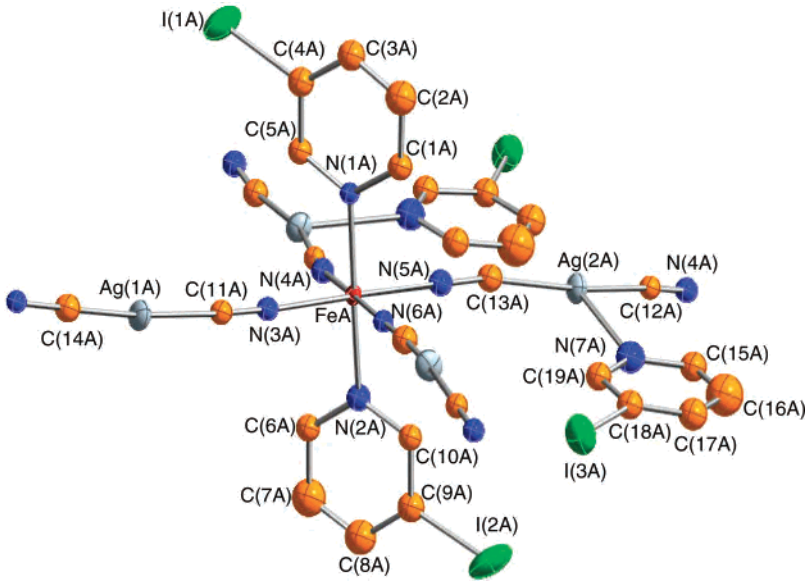

Figure 6. ORTEP representation of a fragment of **6** containing its asymmetric unit and atom numbering. Thermal ellipsoids are presented at 30% probability.

respectively). The separation between two consecutive layers belonging to two different pairs is ca. 6 Å (Figure 5b).

Structure of 6. This compound crystallizes in the noncentrosymmetric $P2_1$ monoclinic space group. It undergoes a spin transition in the temperature range 225−400 K. We have studied the single-crystal X-ray data at 200 K and 270 K where the system is fully in the LS state and almost midway of the HS ↔ LS conversion, respectively. It has been impossible to study the crystal structure at higher temperatures because it deteriorates rapidly.

This compound also consists of slightly corrugated layers; however, in the present case, the layers are not organized by pairs but in a set of equally spaced layers. There are two crystallographically distinct layers whose asymmetric units differ slightly. Each layer is made up only of one crystallographically independent iron(II) site, Fe(A) or Fe(B), which define a distorted [FeN_6] octahedron. Figure 6 displays a fragment of the layer defined by Fe(A) sites. The atom numbering of the layer constituted by Fe(B) sites has been kept identical with that of Fe(A) sites but with the label B instead of A. The axial positions of the [FeN_6] octahedron are occupied by the 3-Ipy ligands while the equatorial positions are occupied by two different bridging anions $[Ag(1)(CN)_2]^-$ and $[Ag(2)(3\text{-Ipy})(CN)_2]^-$. At 270 K, the average Fe−N axial distance is 2.059(8) and 2.065(8) Å, whereas the average equatorial distance is 2.005(14) and 2.026(15) Å for the A and B layers, respectively. At 200 K the Fe−N bond distances are characteristic for the iron(II) ion in the LS state; the average Fe−N distance shortens by 0.069 Å (site A) and 0.080 Å (site B). These values are consistent with the HS-to-LS change of population deduced from the magnetic behavior. The $[Ag(1)(CN)_2]^-$ bond distances and angles are very similar in both kinds of layers and differ very little from linearity; the average C−Ag−C angle is 175.2(9)° at 200 K and 173.3(7)° at 270 K. The in situ formed $[Ag(2)(3\text{-Ipy})(CN)_2]^-$ anion has a strongly distorted trigonal geometry with the C(12)−Ag(2)−C(13), C(12)−Ag(2)−N(7), and C(13)−Ag(2)−N(7) average bond angles equal to 161.3(6)° [161.6(9)°], 100.0(5)° [99.65(7°)], and 98.5(5)° [98.0(8)°] at 270 K [200 K].

Each bridging $[Ag(1)(CN)_2]^-$ and $[Ag(2)(3\text{-Ipy})(CN)_2]^-$ ligand connect two iron atoms forming slightly distorted $\{-Fe[Ag(1)(CN)_2]-Fe-[Ag(2)(3\text{-Ipy})(CN)_2]-\}_2$ squares which share the edges and define a stack of almost identical A and B grids (Figure 7a). The average dimensions of the edges of the square are Fe−Ag(1)−Fe 10.358(3) [10.229(5)] Å and Fe−Ag(2)−Fe 10.293(3) [10.169(5)] Å at 270 [200] K. Two consecutive edges of the square are formed by the same kind of bridge, and the 3-Ipy group coordinated to the Ag(2) atom occupies the center of the window and lies in the plane of the layer (Figure 7a). The 3-Ipy ligand coordinated to the consecutive Ag(2) atom lies in the window defined by the adjacent square. Such disposition of Ag(2)−3-Ipy moieties confers noncentrosymmetry to the crystal. These layers superpose along the [101] direction (Figure 7b). Between the layers (separated by ca. 8.3 Å) there is room to include one guest 3-Ipy molecule, which does not interact significantly with the host layers (Figure 8).

Magnetic Behavior. The thermal dependences of the product $\chi_M T$ for compounds **1**−**3**, **5**, and **6** are displayed in Figure 9, χ_M being the molar magnetic susceptibility and T the temperature. For **1**, $\chi_M T$ is equal to 3.68 cm^3 K mol^{-1} at 300 K, which is in the range of the values expected for an iron(II) ion in the HS state. Upon cooling, $\chi_M T$ remains almost constant down to ca. 230 K; below this temperature $\chi_M T$ decreases more markedly displaying a two-step spin transition with a characteristic plateau centered around 50% of conversion. The critical temperatures are $T^1_{1/2} = 96$ K and $T^2_{1/2} = 162$ K, and the temperature at the middle of the plateau is 127 K. The $\chi_M T$ value drops to 0.45 and 0.18 cm^3 K mol^{-1} at 50 and 5 K, respectively, indicating the occurrence of 5−10% residual paramagnetism. Cooling and warming modes match perfectly indicating that there is no appreciable thermal hysteresis. For **2**, $\chi_M T$ is equal to 3.57 cm^3 K mol^{-1} at 300 K and remains constant down to 115 K; below this temperature, a sharp spin transition involving

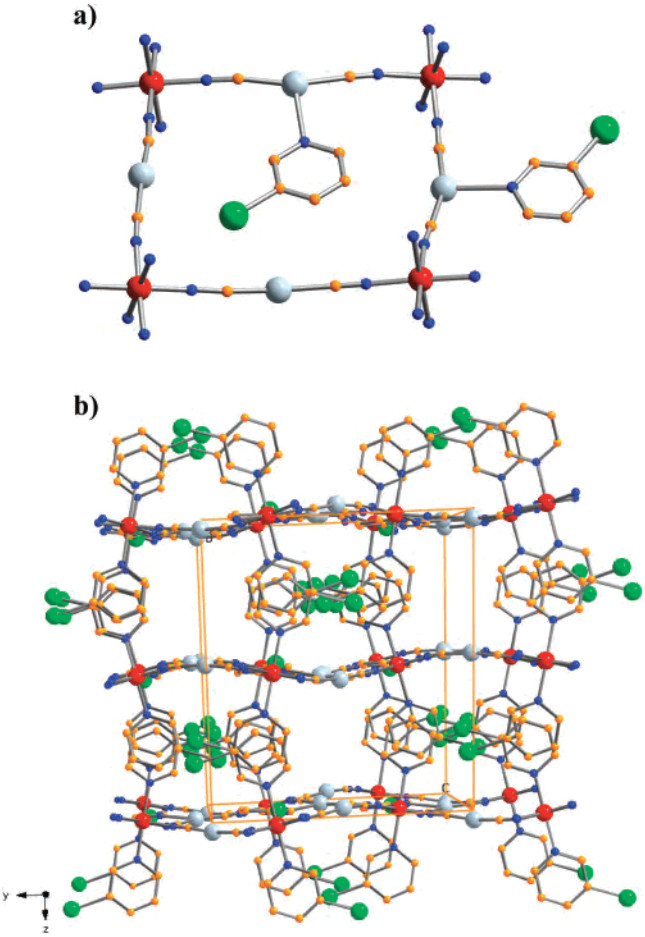

Figure 7. (a) View of a window of the grid of compound **6** emphasizing the 3-Ipy ligand coordinated to the silver atom. (b) Stacking of three consecutive layers of **6** along the [100] direction. (Uncoordinated 3-Ipy molecules have not been included for simplicity.)

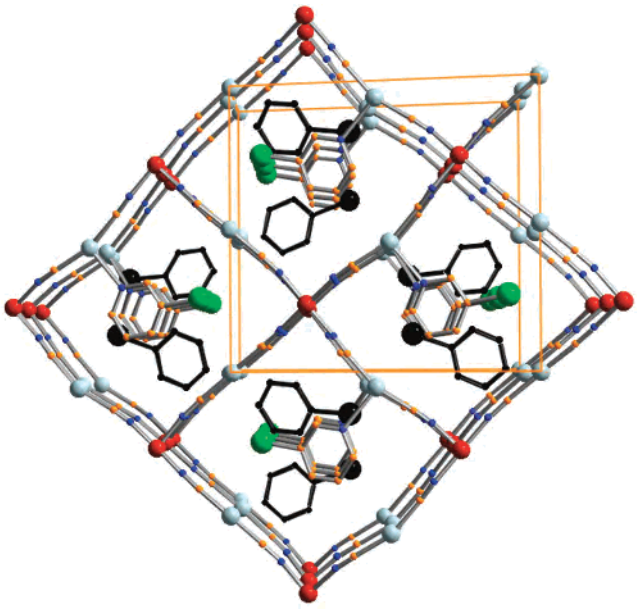

Figure 8. Stacking of three consecutive layers of **6** along the [001] direction. The uncoordinated 3-Ipy ligands are noted in black color.

ca. 50% of HS ↔ LS conversion takes place ($T_{1/2}$ = 106 K). At temperatures lower than 65 K, $\chi_M T$ decreases again due to the occurrence of zero-field splitting (ZFS) of the S = 2 state of the remaining 50% HS species. The spin transition observed for **1** and **2** is accompanied by a drastic and reversible change of color from yellow (HS) to deep red (LS).

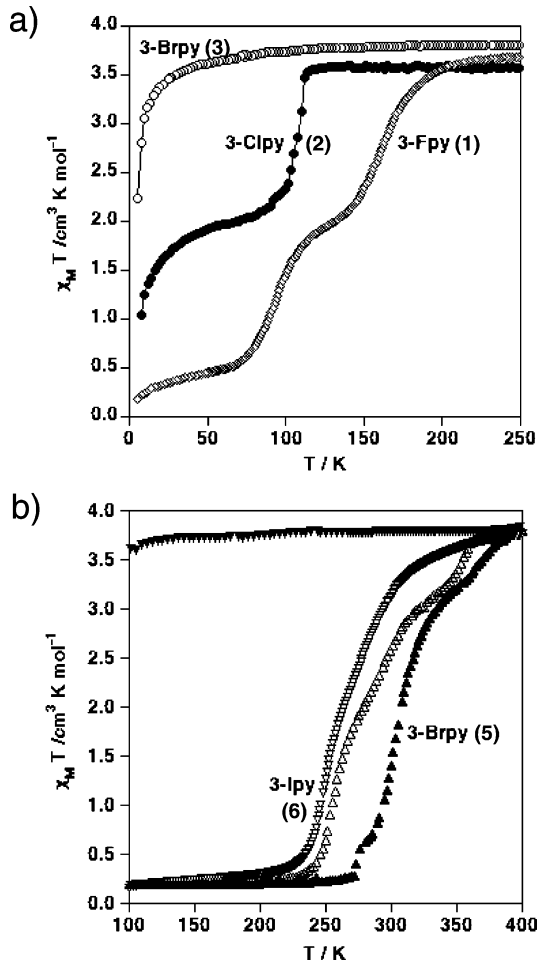

Figure 9. $\chi_M T$ versus T plots for (a) compounds **1**−**3** and (b) compounds **5** and **6**. (Warming and cooling modes during the first cycle are represented by normal and inverted triangles, respectively.)

The magnetic behaviors of **3** and **4** are characteristic of iron(II) compounds in the HS state, $\chi_M T$ = 3.79 cm^3 K mol^{-1} (**3**) and 3.83 cm^3 K mol^{-1} (**4**) at 300 K, displaying ZFS at low temperatures. However, **5** and **6** undergo a spin transition in the temperature range 200−400 K. The $\chi_M T$ is 1.39 cm^3 K mol^{-1} at 300 K for **5**, indicating the occurrence of ca. 63% iron(II) atoms in the LS state. Then, it decreases until 0.28 cm^3 K mol^{-1} at 270 K and the spin conversion is practically complete below this temperature. In the warming mode, $\chi_M T$ increases continuously up to 358 K, and then the slope of the curve increases significantly up to reach a $\chi_M T$ value of 3.80 cm^3 K mol^{-1} at 400 K. The temperature at which the molar fraction of the HS and LS centers is equal to 0.5, $T_{1/2}$, is ca. 306 K. Then, when **5** is cooled from 400 K, it displays a different magnetic behavior. It is no longer a spin-crossover system but shows the typical magnetic properties of an iron(II) ion in the HS state in the whole range of temperatures (2−400 K).

Compound **6** undergoes a similar spin conversion like **5** but slightly shifted to lower temperatures. At 300 K the $\chi_M T$

value is 2.59 cm^3 K mol^{-1} indicating the occurrence of ca. 32% iron(II) centers in the LS state at this temperature. When cooling, it accomplishes the spin conversion with a $\chi_M T$ value of 0.22 cm^3 K mol^{-1} at 210 K. Similarly to **5**, when **6** is warmed it achieves a $\chi_M T$ value of 3.79 cm^3 K mol^{-1} at 400 K. The $T_{1/2}$ value for this transition is 275 K. Another similarity between both compounds is that the magnetic curve is not the same in the cooling mode; however, in the case of **6** the spin transition remains, although slightly shifted to low temperatures, $T_{1/2} \approx 261$ K. This transition does not change after several cooling−warming cycles.

Discussion

This work was undertaken to explore new structural and spin-crossover properties that assemblies of Fe(II), 3-Xpy, and $[Ag(CN)_2]^-$ could afford. Here we have reported the synthesis, crystal structure, and magnetic properties of six new coordination polymers. Polymers **1**−**4** are tightly related from a structural point of view, while **5** and **6**, which are isostructural to each other, present different compositions and structures. The crystal structures of **1**−**6** are made up of layers of $[FeAg(CN)_2]_n$ decorated with 3-Xpy ligands coordinated to the Fe(II) ions. The layers formed by sharing $[FeAg(CN)_2]_4$ squarelike units interact by pairs forming double layers held together by argentophilic interactions. This is an unprecedented result as the present members of the family of compounds $\{Fe(L)_x[Ag(CN)_2]_2\}$ (L = 4,4′-bipyridine, bispyridylethylene, pyrazine, pyrimidine, or 3-CN-pyridine) are single or interpenetrated 3D coordination polymers. In this respect, it deserves to have compounds **1**−**4** compared with $\{Fe(3\text{-CNpyridine})_2[Ag(CN)_2]_2\}\cdot 2/3H_2O$, which only differ in the substitute group bonded in the 3 position of the pyridine. The latter polymer is made up of triple interlocked 3D networks, with the topology of NbO. It undergoes a complete spin transition strongly coupled with modulation of the argentophilic interactions occurring between the different networks.[9d] In contrast to other cases, in which formation of distinct polymorphs was observed depending on the experimental conditions, this compound is the only species formed in the crystallogenesis process. Indeed, the homologous compound $\{Fe(3\text{-CNpy})_2[Au(CN)_2]_2\}\cdot nH_2O$ displays three different polymorphs, one being isostructural to the Ag derivative and the other two corresponding to 2D coordination polymers.[9e] One of these polymorphs presents a structure similar to that observed for **1**−**4**.

As far as the spin-crossover properties are concerned, **1** (3-Fpy) and **2** (3-Clpy) undergo a spin-state change. The former displays a two-step spin conversion reflecting the occurrence of two crystallographically distinct iron(II) sites. Both steps are poorly cooperative. The high-temperature step takes place in an interval of 80 K ($T^{(2)}_{1/2} = 162$ K), while the low-temperature step occurs in an interval of around 60 K ($T^{(1)}_{1/2} = 96$ K). This step occurs at relatively low temperatures being most probably the reason why the $\chi_M T$ values below 70 K are slightly higher than expected because they are frozen in the HS state. The related 2D compound $\{Fe(py)_2[Ag(CN)_2]_2\}$ has been recently reported. It is interesting to note that this compound displays a two-step transition quite similar to that described for **1** with $T^{(2)}_{1/2} = 146.3$ K and $T^{(1)}_{1/2} = 91$ K ($T^{(1)}_{1/2}$ corresponds to the average cooling and warming temperatures).[11] A much steeper conversion is observed for **2**, which is also observed at relative low temperatures ($T_{1/2}$= 106 K). The 50% character of the transition is most likely connected with this fact, given that a further HS-to-LS conversion should be thermally blocked. This magnetic behavior is consistent with the crystal structure at 100 K as the average Fe−N bond distance and the crystal volume change correspond quite well to 50% spin-state conversion for the iron(II) ion. However, despite the high quality of the crystal resolution, only one type of iron(II) site, averaged between the high- and low-spin states, is observed. This is not an uncommon situation in spin-crossover compounds (see for instance refs 9f and 12). Compounds **3** and **4** are fully HS in the whole range of temperatures. Thus, there is a downshift tendency for the critical temperatures as the electronegativity of the halogen atom decreases. Obviously, the critical temperatures for **3** and **4** would be so low that no spin conversion can be expected.

From simple electronic structure considerations, one would expect an opposite trend because the lone electron pair cloud of the nitrogen atom "shrinks" as the electronegativity of the axial ligand 3-Xpy (X = F, Cl, Br, I) increases conferring it a lower donor capability, and consequently, a decrease of the ligand field strength and of the critical temperature should be observed. However, this supposed loss of donor capability of the 3-Xpy ligand is not reflected in the structure as a decrease of the $Fe-N_{axial}$ bond distance is observed when moving from **4** to **1** while the average of the $Fe-N_{equatorial}$ bond distances remain practically identical (within the error limits) for the four compounds. The average $Fe-N_{axial}$ distance is 2.225(5) Å for **1**, 2.244(4) for **2** and **3**, and 2.261(7) Å for **4**. Taking into account that the ligand field strength $10Dq$ is proportional to $(1/R)^6$, where R represents the Fe−N distance, a decrease of the $10Dq_{axial}$ value of ca. 7.4% is observed when moving from **1** to **2** and **3** and an additional decrease of ca. 6.6% when moving from the latter to **4**. These data correlate quite well with the magnetic properties of **1**−**4**.

In a recent paper, Kaizaki and co-workers have discussed the effect of substituted pyridines (Y-py) as axial ligands in the iron(II) dinuclear complexes $\{[Fe(NCX)(Y\text{-py})]_2(\mu\text{-bpypz})_2\}$, where X = S or BH_3, Y-py = 3-Brpy, 3-Clpy, py, 3-Mepy, and 4-NMe_2py, and bpypz is 3,5-bis(2-pyridyl)-pyrazolate. The two halves that constitute the dinuclear species are related by an inversion center. Each half contains an iron atom whose axial positions are occupied by the ligands NCX^- and Y-py. In this series $T_{1/2}$ increases in the following way: 4-Mepy (106 K) < 4-NMe_2py (113 K) < py (129 K) < 3-Mepy (130 K) < 3-Clpy (148 K) < 3-Brpy (158 K). This trend has been justified in terms of π acceptor

(11) Rodriguez-Velamazán, J. A.; Castro, M.; Palacios, E.; Burriel, R.; Kitazawa, T.; Kawasaki, T. *J. Phys. Chem. B* **2007**, *111*, 1256.
(12) Moussa, N. O.; Trzop, E.; Mouri, S.; Zein, S.; Molnár, G.; Gaspar, A. B.; Collet, E.; Buron-Le Cointe, M.; Real, J. A.; Borshch, S.; Tanaka, K.; Cailleau, H.; Bousseksou, A. *Phys. Rev. B* **2007**, *75*, 054101.

properties of the X-py ligands. In fact, a linear correlation between the spin-crossover temperature, $T_{1/2}$, for both types of axial ligands NCX^- and the Hammett constant of the axial Y-py ligands was found.[13]

It is obvious that the general trend found in this series has a direction opposite to that we find for the title compounds. In this respect, the distinct nature of both kinds of solids, namely discrete dinuclear species versus infinite 2D polymers, may play a major role in the characteristic temperature of the transition. Given that close to the "crossing point" the energy gap between the two spin states is very small, the transition temperatures may be dominantly influenced by crystal packing factors. The occurrence of polymorphism in spin-crossover compounds, which present different characteristic temperatures and different spin states displaying exactly the same chemical constituents, is a clear illustration of that.[14]

In this case, there is an apparent correlation between the halogen atom's size and the stabilization of the HS state. The halogen atoms X are located between the double layers, and they interact with each other displaying contacts shorter than the sum of the corresponding van der Waals distances: F···F = 2.312(2) Å, Cl···Cl = 3.440(2) Å, Br···Br = 3.806(2) Å, and I···I = 3.6062(11) Å. These interactions are defined in such a way that one 3-Xpy group of each iron(II) belonging to a layer, i.e., L1, interacts with an equivalent ligand coordinated to an iron(II) atom located in the layer L(1 + 3) for X = Cl, Br, and I. For the F derivative, these interactions occur similarly but involve 50% of the iron atoms (see Supporting Information). A possible explanation for the observed trend could be expressed in terms of the ligand field strength felt by the Fe(II) ions in the crystal, which is the result of the internal pressure generated by the lattice. This pressure can be absorbed more efficiently when highly polarizable atoms are present in the crystal as they can respond more readily to the strain changes in the lattice. This effect has been noted in some experiments performed at high pressures. For instance in the system $[Fe(dppen)_2(X)_2]$ (dppen = *cis*-1,2-bis(diphenylphosphino)ethylene; X = Cl^-, Br^-) both compounds are HS but undergo a spin-state change at high pressures at 300 K. The critical pressure, P_c, at which the Cl derivative displays a spin conversion is 0.8 GPa while in Br it occurs at 6 GPa. This observation has been ascribed in part to the more polarizable character of the Br^- anion.[15] In fact, the 3-Brpy derivative undergoes a thermal spin transition at higher pressures than 1 bar and a similar effect can be expected for the 3-Ipy derivative (see Supporting Information). Hence, although the halogen is not directly bonded to the iron(II) atom, a similar argument can be used for the title compounds in which the internal chemical pressure associated with the lattice could be attenuated more efficiently depending on the polarizability of the halogen atom in the 3-Xpy group. Evidence for the existence of chemical pressure has been given in metal dilution experiments in isostructural matrices[16] or encapsulating a metal complex, susceptible of undergoing spin crossover, in the pores of a 3D network.[17]

The presence of an excess of the 3-Xpy ligand facilitates the formation of compounds **5** and **6**. They are made up of a stacking of 2D coordination polymers. However, these polymers do not define double layers like **1**−**4** and, consequently, no argentophilic interactions are observed. There are two additional 3-Xpy guest molecules in the lattice; one is uncoordinated and located between the layers while the other fits quite well in the windows defined by the $\{Fe[Ag(CN)_2]\}_4$ squares and coordinates one silver atom defining the in situ formed species $[Ag(3\text{-}Xpy)(CN)_2]^-$. The uncoordinated 3-Xpy molecules interact via π-stacking with the coordinated ones to the Fe(II) atom defining infinite chains, and there also are weak X···X contacts between the three types of 3-Xpy molecules. In addition to these important structural differences, another remarkable feature, which differentiates **5** and **6** from the **1**−**4** series, is the short Fe−N distances (observed for the 3-Ipy derivative), indicating that the former are almost fully LS at temperatures close to 300 K. Consequently, the solids are deep red (**5**, **6**) instead of pale yellow (**1**−**4**) at room temperature. These data are in agreement with the magnetic behavior observed for **5** and **6**. At room-temperature both compounds contain a noticeable number of iron(II) ions in the LS state. Furthermore, they change their magnetic properties after reaching 400 K. In the case of **5**, this drastic change is related with the thermal stability as it loses, in two successive steep steps, four 3-Brpy molecules (T_1 = 365 K and T_2 = 404 K). In contrast, a rapid loss of the 3-Ipy molecules takes place in only one step at temperatures higher than 400 K for **6** (see Supporting Information). Therefore, the down-shift temperature observed for the transition of **6** could probably be due to some reorganization of the uncoordinated 3-Ipy molecules in the lattice.

Although it is tempting to make some conjecture about the notable differences in the spin-crossover properties of the two groups of compounds, free guest (**1**−**4**) and guest-loaded (**5**, **6**) derivatives, we consider that the experimental data do not allow us to rationalize these observations.

Acknowledgment. Financial support is acknowledged from the Spanish DGICYT (Grant CTQ 2004-03456) and from the Generalitat Valenciana for the research Grant ACOMP/2007/110.

(13) Nakano, K.; Suemura, N.; Yoneda, K.; Kawata, S.; Kaizaki, S. *Dalton Trans.* 2005, 740.

(14) See, for instance, the following: (a) Ozarowski, A.; McGarvey, B. R.; Sarkar, A. B.; Drake, J. E. *Inorg. Chem.* **1988**, *27*, 628. (b) Gaspar, A. B.; Muñoz, M. C.; Moliner, N.; Ksenofontov, V.; Levchenko, G.; Gütlich, P.; Real, J. A. *Monatsh. Chem.* **2003**, *134*, 285.

(15) McCusker, J. K.; Zvagulis, M.; Drickamer, H. G.; Hendrickson, D. N. *Inorg. Chem*. **1989**, *28*, 1380.

(16) (a) Martin, J.-P.; Zarembowitch, J.; Dworkin, A.; Haasnoot, J. G.; Codjovi, E. *Inorg. Chem.* **1994**, *33*, 2617. (b) Martin, J.-P.; Zarembowitch, J.; Bousseksou, A.; Dworkin, A.; Haasnoot, J. G.; Varret, F. *Inorg. Chem.* **1994**, *33*, 6325. (c) Haddad, M. S.; Federer, W. D.; Lynch, M. W.; Hendrickson, D. N. *J. Am. Chem. Soc.* **1980**, *102*, 1468. (d) Haddad, M. S.; Federer, W. D.; Lynch, M. W.; Hendrickson, D. N. *Inorg. Chem.* **1981**, *20*, 131. (e) Ganguli, P.; Gütlich, P.; Müller, E. W. *Inorg. Chem.* **1982**, *21*, 3429. (f) Sorai, M.; Ensling, J.; Gütlich, P. *Chem. Phys.* **1976**, *18*, 199.

(17) Sieber, R.; Decurtins, S.; Stoeckli-Evans, H.; Wilson, C.; Yufit, D.; Howard, J. A. K.; Capella, S. C.; Hauser, A. *Chem.—Eur. J.* **2000**, *6*, 361.

Supporting Information Available: CIF data for compounds **1**, **2** (at 270 and 100 K), **3**, **4**, and **6**, cell parameters of compound **5**, magnetic behavior of compound **4**, thermal stability of compounds **5** and **6**, crystal packing showing the interlayer interactions through shorter X···X contacts for **1**−**4**, and magnetic properties of **4** at 4.3 kbar. This material is available free of charge via the Internet at http://pubs.acs.org.

IC700607X